

# A multi-probe thermophoretic soot sampling system for high-pressure diffusion flames

Alex M. Vargas and Ömer L. Gülder

*Institute for Aerospace Studies, University of Toronto, Toronto, Ontario M3H 5T6, Canada*

(Received 29 February 2016; accepted 11 April 2016; published online 2 May 2016)

Optical diagnostics and physical probing of the soot processes in high pressure combustion pose challenges that are not faced in atmospheric flames. One of the preferred methods of studying soot in atmospheric flames is *in situ* thermophoretic sampling followed by transmission electron microscopy imaging and analysis for soot sizing and morphology. The application of this method of sampling to high pressures has been held back by various operational and mechanical problems. In this work, we describe a rotating disk multi-probe thermophoretic soot sampling system, driven by a microstepping stepper motor, fitted into a high-pressure chamber capable of producing sooting laminar diffusion flames up to 100 atm. Innovative aspects of the sampling system design include an easy and precise control of the sampling time down to 2.6 ms, avoidance of the drawbacks of the pneumatic drivers used in conventional thermophoretic sampling systems, and the capability to collect ten consecutive samples in a single experimental run. Proof of principle experiments were performed using this system in a laminar diffusion flame of methane, and primary soot diameter distributions at various pressures up to 10 atm were determined. High-speed images of the flame during thermophoretic sampling were recorded to assess the influence of probe intrusion on the flow field of the flame. *Published by AIP Publishing.* [<http://dx.doi.org/10.1063/1.4947509>]

## I. INTRODUCTION

Designing engines to operate mainly in the diffusion mode of combustion makes it possible to have a reliable and consistent combustion process with overall equivalence ratios much lower than the lean flammability limits. These engines are built to operate at high pressures, exceeding 40 atm in gas turbines and 100 atm in diesel engines, for thermal efficiency and compactness concerns. The formation of soot is an artifact of the diffusive combustion process, and the pressure has a significant degree of influence on soot concentrations in diffusion flames.<sup>1</sup> These types of flames in practical engines are not easily characterized because of experimental limitations related to optical accessibility, complex flame geometries, and the vast range of time and length scales.

Since the chemical reactions governing the various flame processes are intrinsically nonlinear, the responses of combustion events to pressure changes are not usually monotonic.<sup>1</sup> Therefore, it is not trivial to scale measurements at atmospheric flames to high-pressure combustion. For this reason, high pressure combustion has been one of the targeted research areas in industry and in academia in recent years.<sup>2,3</sup>

Currently, measurements of spatially and temporally resolved turbulent mixing rates in sooting turbulent diffusion flames are not feasible. Pressure compounds the problem further not only by affecting the soot formation and oxidation rates (mainly through changing the associated time scales) but also by altering the turbulence field and therefore modifying the mixing rates. Through the use of approaches like the flamelet hypothesis, which proposes that turbulent flames are a collection of deformed laminar flames, the similarities between laminar and turbulent flames can be exploited.<sup>4</sup> This

opens the possibility of using laminar diffusion flames in high-pressure experiments for tractable measurements. However, there are relatively few detailed fundamental studies on soot formation in laminar diffusion flames at elevated pressures.<sup>1,5</sup>

Experimental research in laminar diffusion flames under elevated pressures is held back by the complications in designing an experimental apparatus and in operating instruments that require accessibility for intrusive and non-intrusive measurement techniques. In addition, the stability of laminar diffusion flames, especially originating from buoyancy effects, becomes an important issue at elevated pressures due to the increase in Grashof number, which scales with the square of pressure. These impediments have limited the number and the extent of experimental soot studies in laminar diffusion flames at elevated pressures.<sup>1,5,6</sup>

A detailed account of soot formation in laminar diffusion flames under elevated pressures and the intrusive and non-intrusive soot measurement methods is given in a recent review paper.<sup>1</sup> For soot particle size, aggregate size, fractal dimension of the aggregate, and soot concentration in atmospheric flames, laser scattering and extinction techniques have been successfully used.<sup>7–10</sup> Although light extinction and spectrally resolved soot radiation have been used for soot concentration and temperature measurements at high-pressure laminar flames,<sup>11,12</sup> light scattering to determine the soot particle size in high-pressure diffusion flames has not yet been demonstrated. Another optical technique to measure soot particle size and concentration is laser-induced incandescence (LII), which has been successfully used at atmospheric conditions.<sup>13,14</sup> However, the application of LII at high pressures faces several challenges that are not encountered at atmospheric pressure, in both experimental implementation and in the interpretation of the detected signals.<sup>15–17</sup> Recent refinements in the LII

technique as well as in the LII heat transfer models have improved the technique to a certain extent, but it is still not clear whether LII is capable of measuring primary soot size at elevated pressures.<sup>18,19</sup> This uncertainty necessitates the use of physical sampling approaches.

The thermophoretic sampling for soot characterization at atmospheric pressure flames using a pneumatically activated sampling probe was described by Dobbins and Megaridis<sup>20</sup> to provide complementary information to optical techniques. Several thermophoretic sampling and subsequent transmission electron microscopy (TEM) analyses for soot morphology studies in atmospheric flames were reported, see, for example, Köylü *et al.*,<sup>21</sup> Hu *et al.*,<sup>22</sup> and Hu and Köylü.<sup>23</sup> Lee *et al.*<sup>24</sup> proposed an improved sampling system, activated pneumatically similar to that of Dobbins and Megaridis,<sup>20</sup> reducing the intrinsic vibration caused by pneumatic controls. For sampling soot particles from a high-pressure laminar premixed flame, Leschowski *et al.*<sup>25</sup> reported a design that adopted the pneumatically activated sampling systems of Dobbins and Megaridis<sup>20</sup> and Lee *et al.*<sup>24</sup> to high pressures.

Wagner and his co-workers reported some of the earlier primary soot particle size measurements in shock tube pyrolysis<sup>26</sup> and high pressure premixed flames.<sup>27</sup> Analysis by transmission electron microscopy of physically collected soot samples from pyrolysis of selected fuels in shock tube experiments concluded that the pressure does not exhibit a marked influence on particle diameters from 25 to 50 atm.<sup>26</sup> On the other hand, Heiderman *et al.*<sup>27</sup> found that, in rich premixed flames of acetylene and air, the primary particle size decreased with increasing pressure from 30 at 70 atm.

We report a multi-probe thermophoretic soot sampling system fitted into a high-pressure chamber that is capable of producing sooting laminar diffusion flames up to 100 atm. The described system provides an easy and precise means of controlling the soot sampling time. It is capable of collecting ten consecutive samples in a single experimental run. In addition, it does not use pneumatic drivers that are associated with high levels of vibration.<sup>24</sup> Proof of principle experiments completed using this system in a high-pressure laminar methane-air diffusion flame are discussed, and the flame disturbance caused by the sampling probe intrusion into the flame is described.

## II. THERMOPHORETIC SAMPLING SYSTEM DESIGN AND OPERATION

The thermophoretic sampling system was designed with the aim of integrating it into an existing high-pressure combustion chamber and its laminar diffusion flame burner. This high-pressure chamber and the co-flow burner have been described in detail in previous publications highlighting its full experimental capabilities;<sup>28–36</sup> only certain technical features, which are required to describe the thermophoretic sampling system and its operation, will be summarized here. A schematic of the experimental setup is shown in Fig. 1, including the optical soot measurement system and the general layout. A cut-away view of the high-pressure combustion chamber and the main components of the thermophoretic sampling system are shown in Fig. 2.

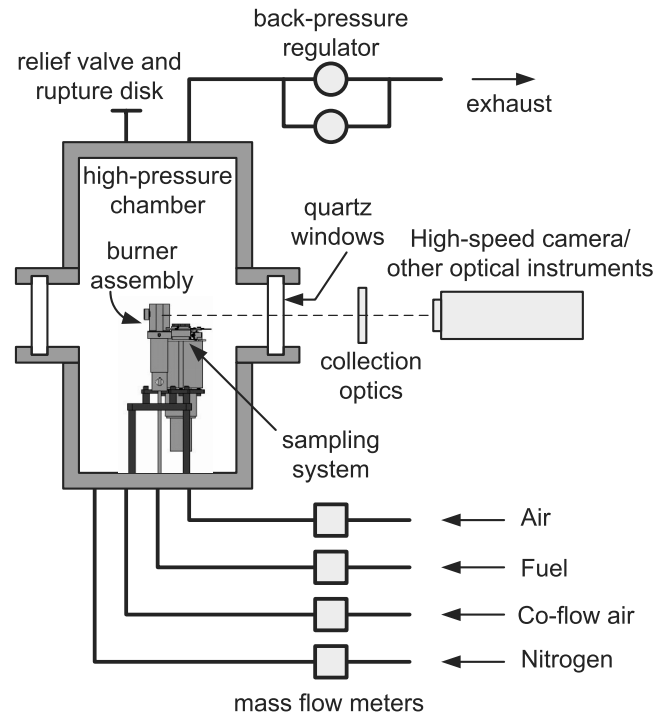


FIG. 1. Schematic of the experimental setup shown with the sampling system in the combustion chamber.

The cylindrical high-pressure chamber's internal diameter and height are 24 and 60 cm, respectively, and it is capable of sustaining operating pressures up to 110 atm. Optical access into the chamber is through three windows located at the chamber mid-height and at angular locations of 0°, 90°, and 180° to allow line-of-sight measurements as well as 90° scattering and imaging experiments. Located in the center of the high-pressure combustion chamber is the co-flow laminar diffusion burner.

The co-flow laminar diffusion type burner consists of a fuel tube concentric with a co-flow air tube. The stainless steel fuel tube has an inner diameter of 3 mm and an outer diameter of 5.7 mm, which decreases with a 14° taper to a fine edge to prevent any recirculation zones from forming at the exit. Located 4 mm upstream from the fuel tube exit is an insert of metal porous material to help minimize non-uniformities in the flow. Encasing the fuel tube is a stainless steel co-flow air tube with an inner diameter that expands from 18 to 38 mm to contain a disk made of porous material, for the same purpose as in the fuel tube, upstream of the co-flow fuel exit. The co-flow burner is enclosed with a flame enclosure to damp the flame instabilities that could be triggered by any recirculation and buoyancy effects present inside the chamber. The flame instabilities are prevalent in atmospheric conditions and have been observed to become stronger at higher pressures leading to flame oscillations. Apart from protecting the flame, the enclosure design serves two different purposes: (i) to hold a ceramic igniter horizontally at 25 mm above the fuel nozzle exit and (ii) to provide physical access to flame via a 3.5 mm thick slot cut perpendicular to the enclosure axis located on the side of the enclosure.

The thermophoretic sampling system, designed and built for soot measurements in the high-pressure chamber described

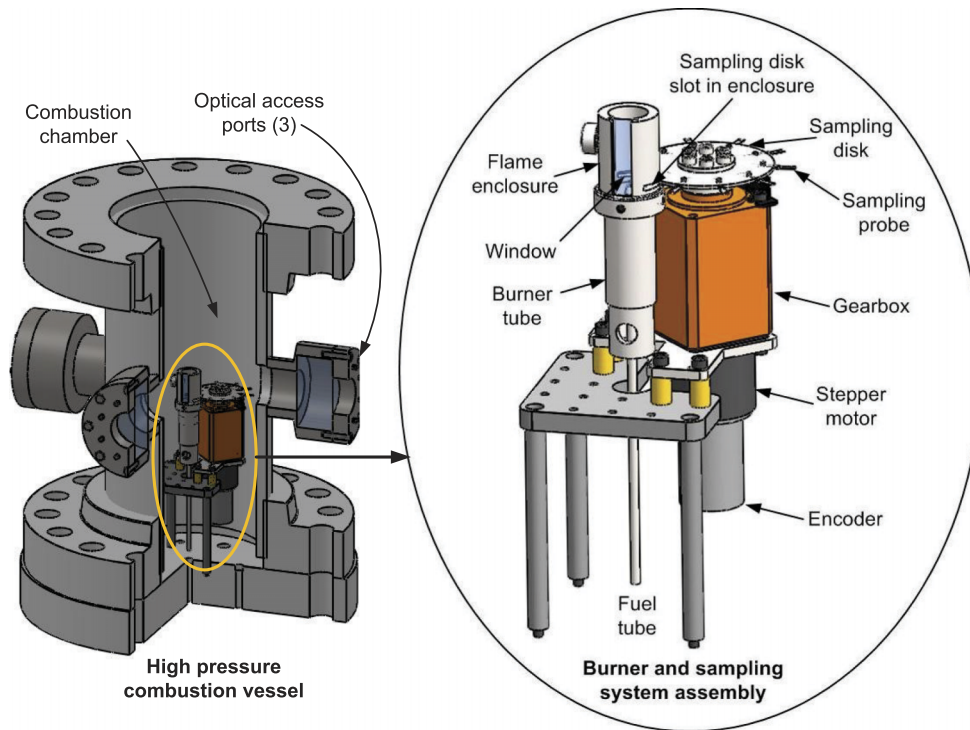


FIG. 2. Cross section of the high-pressure combustion chamber with the thermophoretic sampling system and the burner assembly. The details of the sampling system and the burner assembly are shown in the blowout view on the right.

above, has three main components: a circular sampling disk, a motor drive, and a programmable control unit. The central component of the system is the circular sampling disk that has ten sampling probe arms extending radially outwards as shown in Figs. 3 and 4. The radial extension of each probe arm can be adjusted by  $\pm 1.25$  mm to allow sampling at different radial locations within the flame at a given height above the

burner rim. Each sampling probe arm holds a 3 mm diameter TEM grid in a pocket located at the outer end of the probe arm. These circular pockets are about 3.3 mm in diameter with a depth of 0.5 mm. On the sampling side, a 2.5 mm slot exposes the mesh of the TEM grid to the flame. These probe features are depicted in Fig. 4. TEM grids were secured into the pockets by a high-temperature resistant adhesive tape.

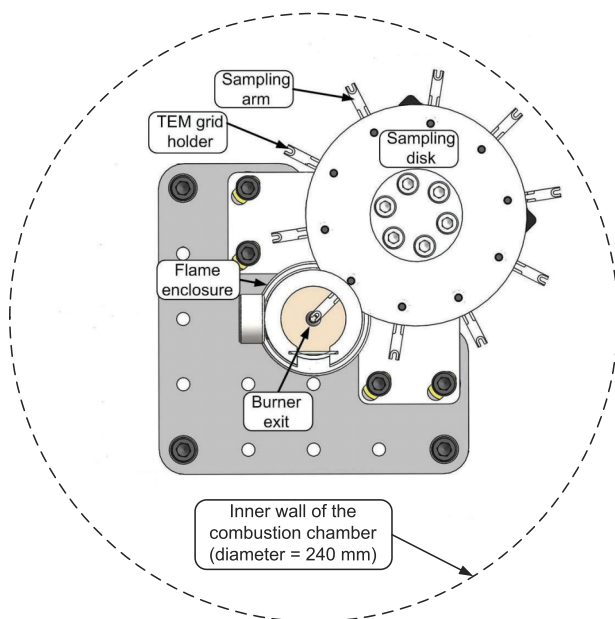


FIG. 3. Top view of the sampling system and the burner with respect to the combustion chamber inner wall. The TEM grid at the end of one of the sampling probe arms is shown concentric with the flame axis.

The motor drive system consists of a stepper motor (Parker, model: OS22B), a gearbox (Parker, model: 10:1-PX23), a rotational encoder (Parker, model: 755A-23A), and a homing limit switch (Crouzet Switches, model: 831860CFD0-BL), Fig. 5. The gearbox used in the motor drive has a ratio of 10:1 and has a custom designed output shaft with a flange for directly connecting the sampling. The motor used is a 0.9° stepper motor with micro-stepping control capability that provides a high angular precision as well as smooth operation. The stepper motor’s output shaft is mounted to the gearbox with a flexible coupler to minimize system vibration. The rotational encoder is connected to the bottom end of the stepper motor, and it tracks the stepper motor displacement to within  $\pm 0.014^\circ$  during the sampling process.

The sampling velocity profile of the TEM grid through the flame cross section of a given height above the burner rim is controlled by the programmable control unit of the sampling system. So the sampling time, i.e., the period during which the TEM grid is exposed to the flame, and the velocity of the sampling arm can be programmed as desired. For example, the control unit can be programmed such that the probe arm would decelerate as it enters the flame and reach a zero velocity when the TEM grid is at the desired sampling location within the flame. At the end of the programmed sampling time, the probe accelerates and exits the flame. The control unit

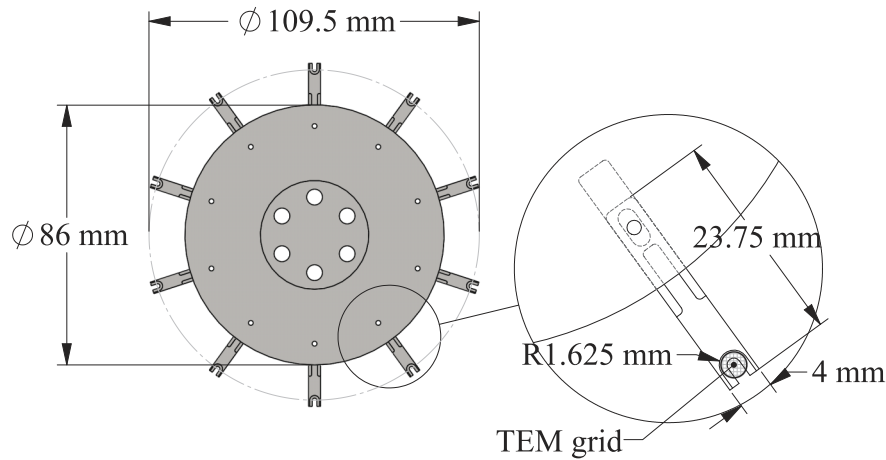


FIG. 4. Details of the sampling disk and TEM probe arms.

can also be programmed so that the probe arm would sweep across the flame cross section at a constant angular velocity for cases in which information averaged over the flame cross section is desired. When the sampling process is initiated, the stepper motor drives the sampling disk at the desired velocity profile and the sampling probe arms rotate through the slot in the flame enclosure. After each probe arm completes the sampling process, the sampling disk is slowed down or brought to a complete stop to allow the flame to recover from the disturbance and to have a stable flame for the next sampling process. To collect samples from different elevations within the flame, the flame enclosure is vertically adjusted to the desired height.

The diameter of the flames is typically in the order of a few millimeters and decreases with increasing pressure<sup>1</sup> in laminar diffusion flames that can be stabilized in the high-pressure combustion chamber. Sampling soot at a given height of the flame with a small TEM grid of 3 mm diameter at a constant angular velocity would yield an averaged soot property at that flame height over the flame diameter. All measurements reported here were made at a height of 3 mm above the burner

rim as it is in the soot formation dominated part of the flame and it is just before the soot yield reaches a maximum.<sup>12,28</sup>

The sampling time should be carefully controlled to avoid too many soot particles collected on the TEM grid forming several layers. In previous studies of soot by thermophoretic sampling and TEM analysis, it was suggested that the ratio of soot covered area to grid surface area should be less than 15%<sup>20,24</sup> for an unbiased analysis of the images. A series of preliminary sampling experiments was conducted to determine the suitable sampling times so that the area coverage would be less than 15% at different pressures. For the case that the sampling probe swipes through the flame at a constant angular velocity, the sampling time is defined as the time it takes for the probe to traverse the diameter of the flame at the sampling height. For the laminar diffusion flames probed in this work, sampling times of 3-8 ms gave satisfactory results. Shortest sampling time with the current design of the motor drive was 2.6 ms with constant angular velocity sampling in the current methane diffusion flames.

### III. DISTORTION OF THE FLAME BY SAMPLING PROBE

Insertion of a physical probe into the flame interferes with the flow field and distorts the streamlines. This interference is one of the major drawbacks of the thermophoretic sampling technique. It is usually assumed that<sup>24</sup> the interference would be mostly hydrodynamic, but still the resulting change in the flow field has the potential to influence the sampling process. It would be quite challenging to quantify the influence of the flow field disturbance on the sampling process; however, high-speed images may provide some insight, although qualitative in nature, into this concern.

We recorded high-speed video images of the flame at 5000 frames/s using a high-frame rate camera (Photron, model: SA5) during the sampling process. A series of images thus captured displays the extent of typical disturbance induced by the sampling probe, Fig. 6. The image A in Fig. 6 is that of the stable flame before sampling starts. The condition that the edge of the thermophoretic probe is about to enter the flame is depicted as image B in Fig. 6. When the probe's

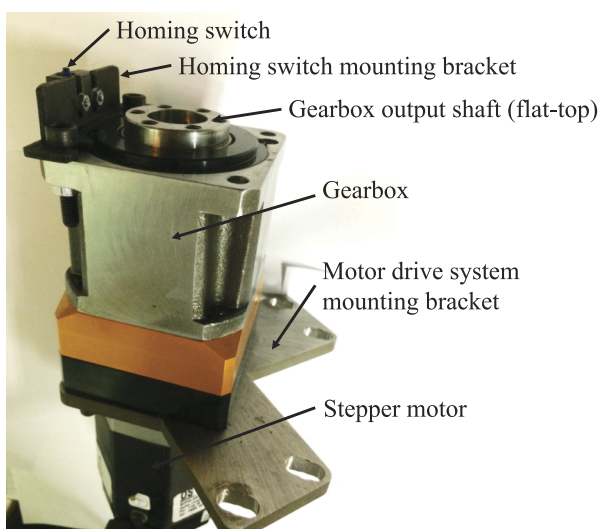


FIG. 5. Picture of the motor drive system.

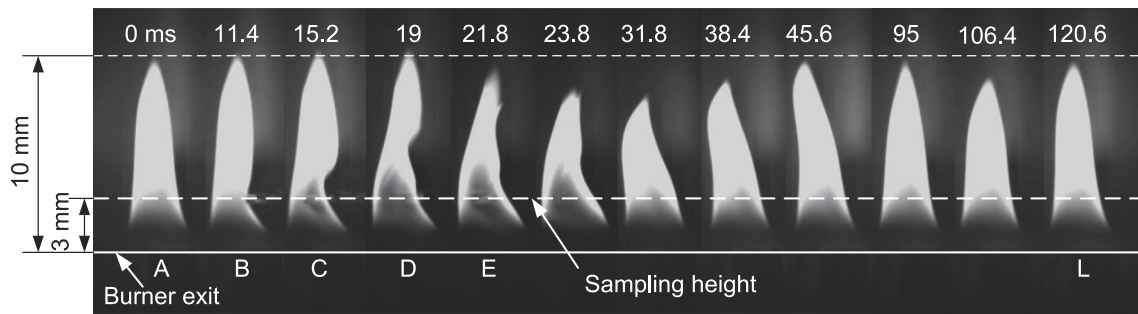


FIG. 6. A series of high-speed images displaying the disturbance induced by the sampling probe at 7.1 atm. The image A shows an undisturbed flame about 11.4 ms before the probe enters the flame. The image B shows the flame when the leading edge of the probe is about to enter the flame. In image C, the TEM grid is concentric with the flame centerline, and in image D, the trailing edge of the probe is just leaving the flame boundary. Subsequent images, E to L, show the various stages of flame's disturbed flow field, and the image L depicts a stable flame again about 110 ms after the sampling probe enters the flame.

leading edge reaches the flame's visible boundary, the flame is slightly distorted due to presence of the probe, image B. When the TEM grid on the probe is concentric with the flame centerline, image C, the distortion caused by the insertion of the sampling probe looks like an indentation on the right side of the flame image. When the trailing edge of the probe is leaving the flame boundary, image D, the flame seems to be already recovering from the distortion, which has moved downstream of the sampling height. The time from the moment the probe's leading edge just entering the flame to the moment its trailing edge leaving the flame is about 7.6 ms. At 3 mm above the burner, the axial velocity along the flame centerline is about 0.5 m/s,<sup>31</sup> whereas the linear velocity of the probe corresponding to a 7.6 ms sampling time is about 0.4 m/s, which is on the same order of magnitude as the flame centerline velocity. Subsequent images show the various stages of the flame's disturbed flow field. The last image in Fig. 6 shows a stable flame about 100 ms after the sampling probe exits the flame.

Lee *et al.*<sup>24</sup> identified the vibration and the aspect ratio of the probe as the major causes of sampling errors in thermophoretic soot collection. The origin of the vibration is due to the pneumatic actuation mechanism they used in their design to deploy the probe into the sampling location. To avoid the vibration problem, our design used a rotating system of probes tightly controlled by a stepper motor. Lee *et al.*<sup>24</sup>

recommended using a probe with an aspect ratio (thickness to width ratio) larger than 0.2, and the probe used in the present design has an aspect ratio of 0.25.

The disturbance caused by the sampling probe has been found to be repeatable, at least in visual appearance, at different pressures and sampling times as depicted in Fig. 7.

#### IV. TEM IMAGE ANALYSIS RESULTS

Soot samples were collected on TEM grids (carbon coated copper grids, SPI:3520C-CF) at various pressures in a methane-air diffusion flame using the thermophoretic sampling system described in Section II. To keep measurements at different pressures tractable, fuel and air mass flow rates were kept constant at all pressures considered. The methane flow rate at all pressure levels was kept as 0.55 mg/s, which corresponds to a carbon mass flow rate of 0.41 mg/s. This carbon flow rate is the same as the carbon flow rates in our previous work with methane and other gaseous<sup>12,28,32</sup> and liquid fuels.<sup>34</sup> At all pressures, a constant co-flow air mass flow of 0.34 g/s is provided. Typical images, recorded by a TEM (Hitachi, model: H-7000), of the collected soot aggregates at various pressures are shown in Fig. 8. The analysis technique described by Lapuerta *et al.*<sup>37</sup> was used to obtain primary soot particle sizes from TEM images.

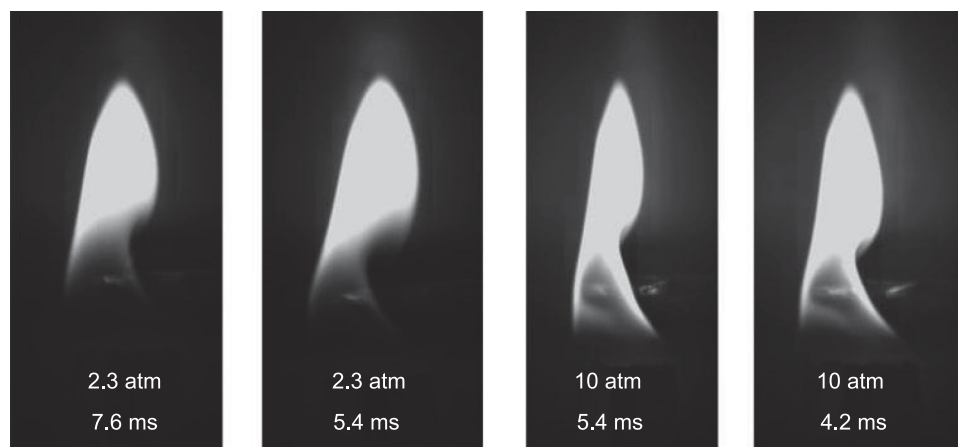


FIG. 7. Flame shape distortion at different pressures and residence times when the TEM grid is concentric with the fuel nozzle of the burner.

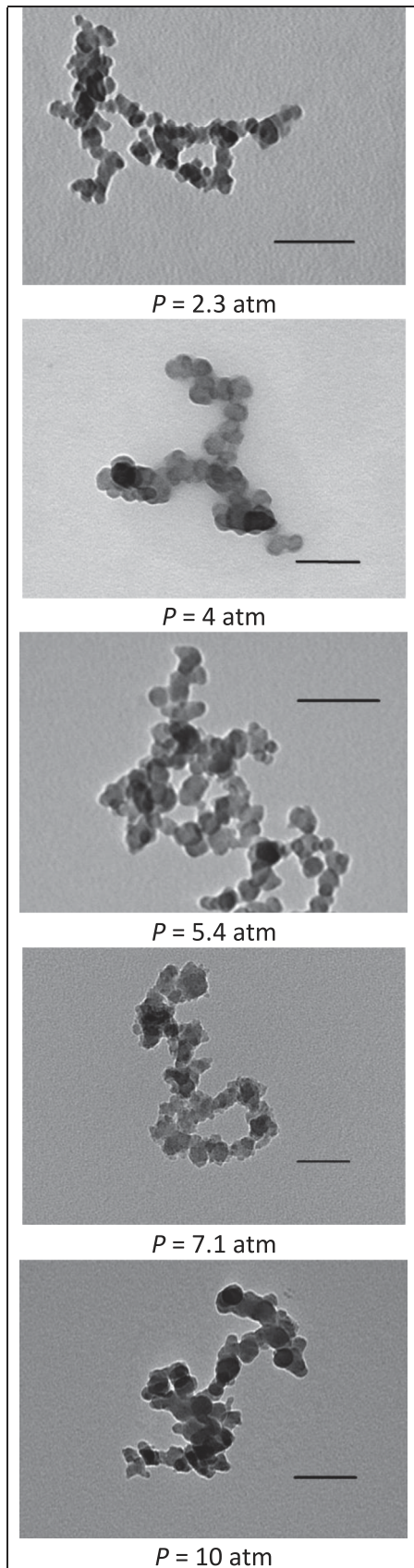


FIG. 8. TEM image of soot aggregate particles at 2.3 atm, 4 atm, 5.4 atm, 7.1 atm, and 10 atm. Solid bars on the images represent 100 nm.

It should be emphasized that the flame heights in buoyancy-dominated laminar co-flow diffusion flames are

independent of pressure and they remain constant when the fuel mass flow rate is kept fixed. Constant flame height with pressure implies that the residence times are independent of the pressure, and measurements can be compared at the same heights above the burner exit.<sup>1</sup> The flames probed in this study are all with the same mass flow rate of methane, and they are buoyancy dominated.<sup>31</sup> Thus, the measurements at the same elevation at different pressures represent the identical residence times for all flames and they can be compared to assess the influence of pressure.

Histograms of primary soot particles determined from TEM images of the soot samples collected at 2.3, 4, 5.4, 7.1, and 10 atm display distributions similar to ones obtained at atmospheric pressure, Fig. 9. These histograms of primary soot particle sizes at various pressures can be fitted with log-normal distribution functions (not shown in Fig. 9) similar to size distributions reported previously for flames at atmospheric conditions.

The overall trend observed from the primary soot diameter distributions shown in Fig. 9 is that the mean primary soot diameter decreases with increasing pressure within the pressure range investigated. Using an identical burner and chamber, Thomson *et al.*<sup>15</sup> measured an “effective primary particle size,” which increased with pressure, using LII. However, as the authors<sup>15</sup> indicated, the effective primary particle size measured by LII at elevated pressures does not represent the primary soot particle diameter because the shielding effect on heat conduction between aggregated particles and the surrounding gas is neglected.<sup>13</sup> As a result, it is not possible to determine whether a change in measured effective particle diameter is caused by a variation of the primary soot particle size, aggregate characteristics, or both without complementary experiments such as thermophoretic sampling. For this reason, it is not possible to compare the current thermophoretic measurements with those performed by LII under comparable conditions.

## V. MEASUREMENT UNCERTAINTIES

Uncertainties involved in the primary soot particle size measurements with the described sampling system and TEM image analysis stem from several factors. One of these factors is related to the intrusive sampling system that disturbs the flow field and could influence the sampling process, as discussed in Section III, and it is difficult to assess its magnitude. Further, radial temperature gradients in co-flow laminar diffusion flames are significant and this may influence the thermophoretic velocity and hence the deposition rates leading to a sampling biased toward hotter regions of the flame. However, the quantification of this bias is beyond the scope of the current study and would require a detailed simulation of the flow and temperature fields of the flame during sampling.

Another source of uncertainty is due to manual analysis of the TEM images to infer the primary soot size distributions. If a statistically sufficient number of samples are available, the error involved was estimated as about 10% (within 95% confidence).<sup>22</sup>

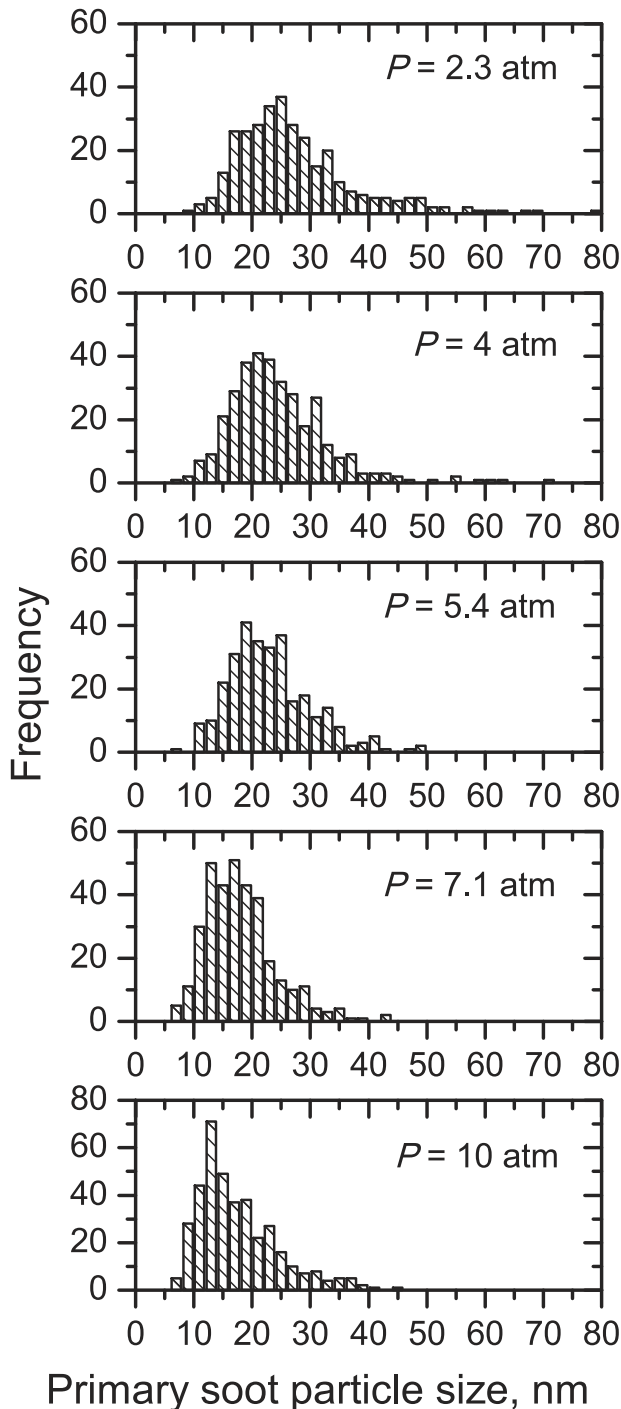


FIG. 9. Variation of the primary soot particle diameter distribution with pressure at a height of 3 mm above the burner exit.

Another potential source of error could be due to the sampling time. This aspect of the problem has been investigated with a limited number of samples to see whether the sampling time, within the limits determined by the preliminary experiments discussed in Section II, affects the measurements significantly. A representative sample of these measurements is shown in Fig. 10. Within the sampling time ranging from 4.2 ms to 7.6 ms, the primary soot size distribution from a flame at 2.3 atm did not change significantly. Similar results were obtained at higher pressures.

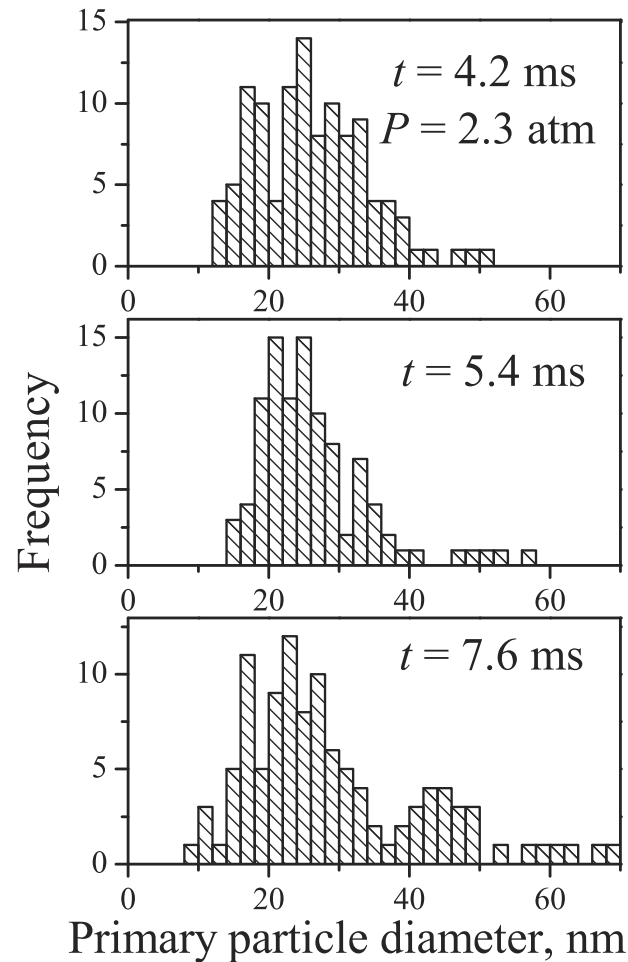


FIG. 10. Primary soot particle size measurements with different sampling times at 2.3 atm.

## VI. CONCLUDING REMARKS

We developed and built an innovative thermophoretic soot sampling system capable of operating at elevated pressures to probe laminar diffusion flames for soot formation studies at high pressures. The sampling system's main component is a rotating disk with multiple probes that can collect samples on TEM grids. The rotating sampling disk is driven by a micro-step stepper motor whose radial displacement is tracked by a rotational encoder. Sampling time and time lag between successive samplings can be programmed with a control unit with high precision. Sampling times as short as 2.6 ms can be achieved at elevated pressures. We used this thermophoretic sampling system in a high-pressure combustion chamber capable of 110 atm with a co-flow laminar diffusion flame burner that was used previously for high-pressure soot studies. We probed a laminar methane diffusion flame up to 10 atm for proof-of-principle measurements and collected soot samples on TEM grids for subsequent TEM imaging and analysis to infer primary soot particle diameters. Soot primary particle size distributions at different pressures showed that mean primary soot diameter decreases with increasing pressure. We recorded high-frame rate images (5000 frames/s) of the flame during the sampling process to assess the influence of probe's intrusion into the flame on the flow field. We demonstrated that

the described thermophoretic sampling system is well suited for high pressure soot research as a complementary method to non-intrusive techniques.

## ACKNOWLEDGMENTS

The authors acknowledge the financial support from Natural Sciences and Engineering Research Council of Canada through Discovery (No. 251116-2012) and Research Tools and Instruments (No. RTI-275925504) grants to the senior author.

- <sup>1</sup>A. E. Karataş and Ö. L. Gülder, "Soot formation in high pressure laminar diffusion flames," *Prog. Energy Combust. Sci.* **38**, 818–845 (2012).
- <sup>2</sup>S. D. Tse, Z. Delin, and C. K. Law, "Optically accessible high-pressure combustion apparatus," *Rev. Sci. Instrum.* **75**(1), 233–239 (2004).
- <sup>3</sup>P. H. Joo, J. Gao, Z. Li, and M. Aldén, "Experimental apparatus with full optical access for combustion experiments with laminar flames from a single circular nozzle at elevated pressures," *Rev. Sci. Instrum.* **86**, 035115 (2015).
- <sup>4</sup>C. H. Kim, F. Xu, and G. M. Faeth, "Soot surface growth and oxidation at pressures up to 8.0 atm in laminar nonpremixed and partially premixed flames," *Combust. Flame* **152**(3), 301–613 (2008).
- <sup>5</sup>M. D. Smooke, M. B. Long, B. C. Connelly, M. B. Colket, and R. J. Hall, "Soot formation in laminar diffusion flames," *Combust. Flame* **143**, 613–628 (2005).
- <sup>6</sup>J. S. McArragher and K. J. Tan, "Soot formation at high-pressures: A literature review," *Combust. Sci. Technol.* **5**, 257–261 (1972).
- <sup>7</sup>C. M. Sorensen, J. Cai, and N. Lu, "Test of static structure factors for describing light scattering from fractal soot aggregates," *Langmuir* **8**, 2064–2069 (1992).
- <sup>8</sup>C. M. Sorensen, J. Cai, and N. Lu, "Light-scattering measurements of monomer size, monomer per aggregate, and fractal dimension for soot aggregates in flames," *Appl. Opt.* **31**(30), 6547–6557 (1992).
- <sup>9</sup>R. Puri, T. F. Richardson, and R. J. Santoro, "Aerosol dynamic processes of soot aggregates in a laminar ethene diffusion flame," *Combust. Flame* **92**, 320–333 (1993).
- <sup>10</sup>Ü. Ö. Köylü and G. M. Faeth, "Spectral extinction coefficients of soot aggregates from turbulent diffusion flames," *J. Heat Transfer* **118**(2), 415–421 (1996).
- <sup>11</sup>D. R. Snelling, K. A. Thomson, G. J. Smallwood, Ö. L. Gülder, E. J. Weckman, and R. A. Fraser, "Spectrally resolved measurements of flame radiation to determine soot temperature and concentration," *AIAA J.* **40**, 1789–1795 (2002).
- <sup>12</sup>K. A. Thomson, Ö. L. Gülder, E. J. Weckman, R. A. Fraser, G. J. Smallwood, and D. R. Snelling, "Soot concentration and temperature measurements in co-annular, non-premixed CH<sub>4</sub>/air laminar flames at pressures up to 4 MPa," *Combust. Flame* **140**, 222–232 (2005).
- <sup>13</sup>D. R. Snelling, F. Liu, G. J. Smallwood, and Ö. L. Gülder, "Determination of the soot absorption function and thermal accommodation coefficient using low-fluence LII in a laminar coflow ethylene diffusion flame," *Combust. Flame* **136**, 180–190 (2004).
- <sup>14</sup>D. R. Snelling, G. J. Smallwood, F. Liu, and Ö. L. Gülder, "A calibration-independent laser-induced incandescence technique for soot measurement by detecting absolute light intensity," *Appl. Opt.* **44**(31), 6773–6785 (2005).
- <sup>15</sup>K. A. Thomson, D. R. Snelling, G. J. Smallwood, and F. Liu, "Laser induced incandescence measurements of soot volume fraction and effective particle size in a laminar co-annular non-premixed methane/air flame at pressures between 0.5–4.0 MPa," *Appl. Phys. B: Lasers Opt.* **83**, 469–475 (2006).
- <sup>16</sup>M. Leschowski, T. Dreier, and C. Schulz, "A standard burner for high pressure laminar premixed flames: Detailed soot diagnostics," *Z. Phys. Chem.* **229**(5), 781–805 (2015).
- <sup>17</sup>E. Cenker, G. Bruneaux, T. Dreier, and C. Schulz, "Sensitivity analysis for soot particle size imaging with laser-induced incandescence at high pressure," *Appl. Phys. B: Lasers Opt.* **119**, 745–763 (2015).
- <sup>18</sup>M. Hofmann, B. F. Kock, T. Dreier, H. Jander, and C. Schulz, "Laser-induced incandescence for soot particle sizing at elevated pressure," *Appl. Phys. B: Lasers Opt.* **90**(3–4), 629–639 (2008).
- <sup>19</sup>M. Charwath, R. Suintz, and H. Bockhorn, "Constraints of two-colour TiRe-LII at elevated pressures," *Appl. Phys. B: Lasers Opt.* **104**, 427–438 (2011).
- <sup>20</sup>R. A. Dobbins and C. M. Megaridis, "Morphology of flame-generated soot as determined by thermophoretic sampling," *Langmuir* **3**, 254–259 (1987).
- <sup>21</sup>Ü. Ö. Köylü, C. S. McEnally, D. E. Rosner, and L. D. Pfefferle, "Simultaneous measurements of soot volume fraction and particle size/microstructure in flames using a thermophoretic sampling technique," *Combust. Flame* **110**, 494–507 (1997).
- <sup>22</sup>B. Hu, B. Yang, and Ü. Ö. Köylü, "Soot measurements at the axis of an ethylene/air non-premixed turbulent jet flame," *Combust. Flame* **134**, 93–106 (2003).
- <sup>23</sup>B. Hu and Ü. Ö. Köylü, "Size and morphology of soot particulates sampled from a turbulent nonpremixed acetylene flame," *Aerosol Sci. Technol.* **38**, 1009–1018 (2004).
- <sup>24</sup>J. Lee, I. Altman, and M. Choi, "Design of thermophoretic probe for precise particle sampling," *J. Aerosol Sci.* **39**(5), 418–431 (2008).
- <sup>25</sup>M. Leschowski, T. Dreier, and C. Schulz, "An automated thermophoretic soot sampling device for laboratory-scale high-pressure flames," *Rev. Sci. Instrum.* **85**, 045103 (2014).
- <sup>26</sup>St. Baurle, Y. Karasevich, St. Slavov, D. Tanke, M. Tappe, Th. Thienel, and H. Gg. Wagner, "Soot formation at elevated pressures and carbon concentrations in hydrocarbon pyrolysis," *Proc. Combust. Inst.* **25**, 627–634 (1994).
- <sup>27</sup>Th. Heiderman, H. Jander, and H. Gg. Wagner, "Soot particles in premixed C<sub>2</sub>H<sub>4</sub>-air flames at high pressures (p=30–70 bar)," *Phys. Chem. Chem. Phys.* **1**(15), 3497–3502 (1999).
- <sup>28</sup>H. I. Joo and Ö. L. Gülder, "Soot formation and temperature field structure in co-flow laminar methane-air diffusion flames at pressures from 10 to 60 atm," *Proc. Combust. Inst.* **32**, 769–775 (2009).
- <sup>29</sup>Ö. L. Gülder, G. Intasopa, H. I. Joo, P. M. Mandatori, D. S. Bento, and M. E. Vaillancourt, "Unified behaviour of maximum soot yields of methane, ethane and propane laminar diffusion flames at high pressures," *Combust. Flame* **158**, 2037–2044 (2011).
- <sup>30</sup>H. I. Joo and Ö. L. Gülder, "Experimental study of soot and temperature field structure of laminar co-flow ethylene-air diffusion flames with nitrogen dilution at elevated pressures," *Combust. Flame* **158**, 416–422 (2011).
- <sup>31</sup>M. R. J. Charest, H. I. Joo, Ö. L. Gülder, and C. P. T. Groth, "Experimental and numerical study of soot formation in laminar ethylene diffusion flames at elevated pressures from 10 to 35 atm," *Proc. Combust. Inst.* **33**(1), 549–557 (2011).
- <sup>32</sup>P. M. Mandatori and Ö. L. Gülder, "Soot formation in laminar ethane diffusion flames at pressures from 0.2 to 3.3 MPa," *Proc. Combust. Inst.* **33**, 577–584 (2011).
- <sup>33</sup>P. H. Joo and Ö. L. Gülder, "Formation of liquid methane water mixture during combustion of a laminar methane jet at supercritical pressures," *Energy Fuels* **26**, 5462–5467 (2012).
- <sup>34</sup>A. E. Karataş, G. Intasopa, and Ö. L. Gülder, "Sooting behaviour of *n*-heptane laminar diffusion flames at high pressures," *Combust. Flame* **160**, 1650–1656 (2013).
- <sup>35</sup>P. H. Joo, M. R. J. Charest, C. P. T. Groth, and Ö. L. Gülder, "Comparison of structures of laminar methane-oxygen and methane-air diffusion flames from atmospheric to 60 atm," *Combust. Flame* **160**, 1990–1998 (2013).
- <sup>36</sup>F. Liu, A. E. Karataş, Ö. L. Gülder, and M. Gu, "Numerical and experimental study of the influence CO<sub>2</sub> and N<sub>2</sub> dilution on soot formation in laminar coflow C<sub>2</sub>H<sub>4</sub>/air diffusion flames at pressures between 5 and 20 atm," *Combust. Flame* **162**(5), 2231–2247 (2015).
- <sup>37</sup>M. Lapuerta, F. J. Martos, and J. M. Herreros, "Effect of engine operating conditions on the size of primary particles composing diesel soot agglomerates," *J. Aerosol Sci.* **38**, 455–466 (2007).